第127巻　第12号　2019年12月 1 日発行（毎月1回1日発行）　ISSN 1348-6535 CODEN:JCSJEW

JCS-Japan

December

vol.127

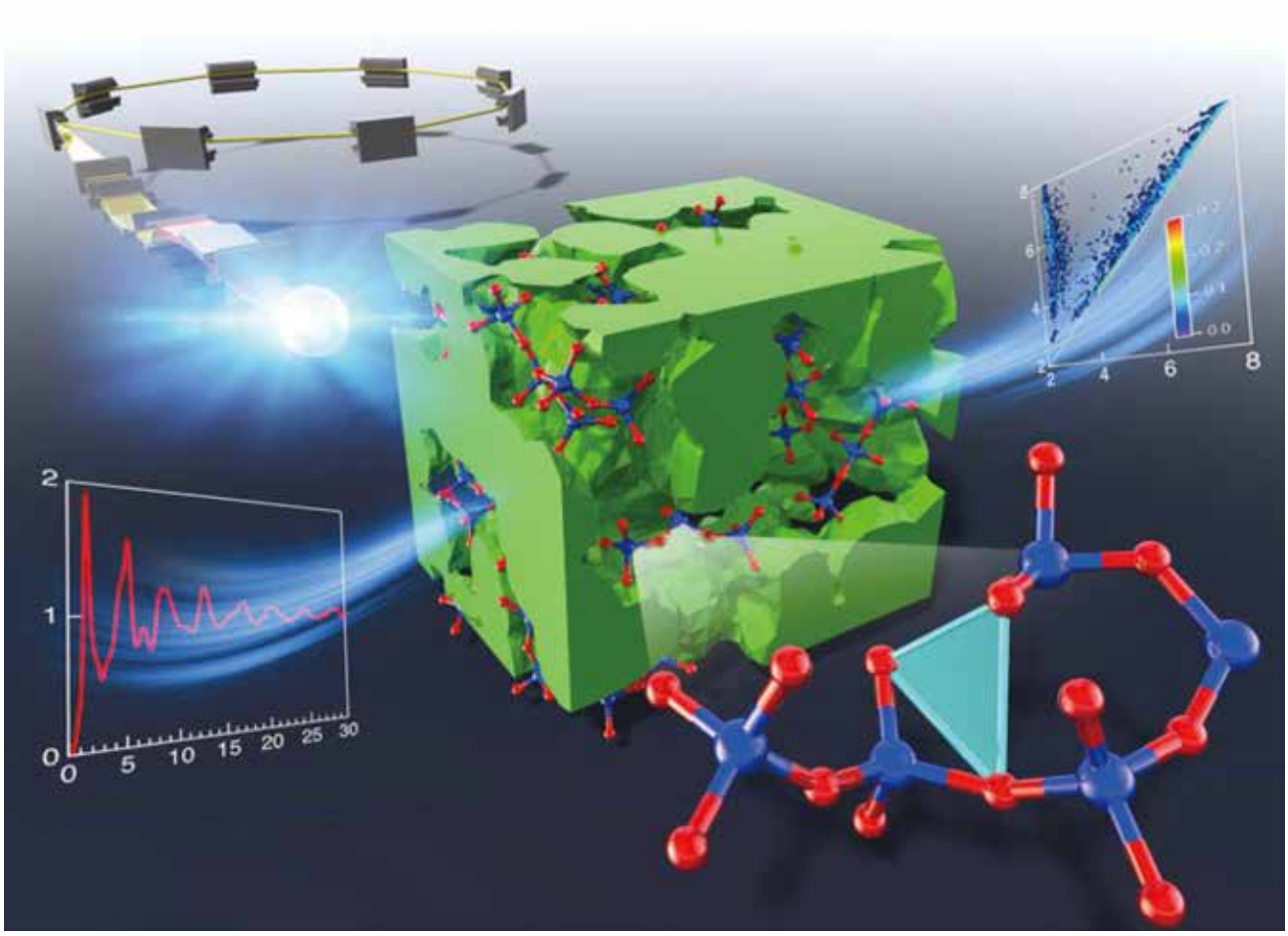

Journal of the Ceramic Society of Japan

2019

Journal of the Ceramic Society of Japan 127 [12] 853-863 2019
DOI http://doi.org/10.2109/jcersj2.19143

JCS-Japan

FULL PAPER

Understanding diffraction patterns of glassy, liquid and amorphous materials via persistent homology analyses

Yohei ONODERA[1,2], Shinji KOHARA[2,3,4,5,6,†], Shuta TAHARA[2,7], Atsunobu MASUNO[2,8], Hiroyuki INOUE[9], Motoki SHIGA[6,10], Akihiko HIRATA[11,12,13,14], Koichi TSUCHIYA[15], Yasuaki HIRAOKA[2,14,16,17], Ippei OBAYASHI[17], Koji OHARA[5], Akitoshi MIZUNO[18] and Osami SAKATA[3,4]

[1]Institute for Integrated Radiation and Nuclear Science, Kyoto University, 2–1010 Asashiro-nishi, Kumatori-cho, Sennan-gun, Osaka 590–0494, Japan
[2]Center for Materials Research by Information Integration (CMI^2), Research and Services Division of Materials Data and Integrated System (MaDIS), National Institute for Materials Science (NIMS), 1–2–1 Sengen, Tsukuba, Ibaraki 305–0047, Japan
[3]Research Center for Advanced Measurement and Characterization, National Institute for Materials Science (NIMS), 1–1–1 Kouto, Sayo-cho, Sayo-gun, Hyogo 679–5148, Japan
[4]Synchrotron X-ray Station at SPring-8, Research Network and Facility Services Division, National Institute for Materials Science, 1–1–1 Kouto, Sayo, Hyogo 679–5148, Japan
[5]Diffraction and Scattering Division, Japan Synchrotron Radiation Research Institute, 1–1–1 Kouto, Sayo, Hyogo 679–5198, Japan
[6]PRESTO, Japan Science and Technology Agency, 4–1–8 Honcho, Kawaguchi, Saitama 332–0012, Japan
[7]Faculty of Science, University of the Ryukyus, 1 Senbaru, Nishihara-cho, Nakagami-gun, Okinawa 903–0213, Japan
[8]Graduate School of Science and Technology, Hirosaki University, 3 Bunkyo-cho, Hirosaki, Aomori 036–8561, Japan
[9]Institute of Industrial Science, The University of Tokyo, 4–6–1 Komaba, Meguro, Tokyo 153–8505, Japan
[10]Department of Electrical, Electronic and Computer Engineering, Faculty of Engineering, Gifu University, 1–1 Yanagido, Gifu 501–1193, Japan
[11]Department of Materials Science, Waseda University, 3–4–1 Ohkubo, Shinjuku, Tokyo 169–8555, Japan
[12]Kagami Memorial Research Institute for Materials Science and Technology, Waseda University, 2–8–26 Nishiwaseda, Shinjuku, Tokyo 169–0051, Japan
[13]Mathematics for Advanced Materials-OIL, AIST, 2–1–1 Katahira, Aoba-ku, Sendai 980–8577, Japan
[14]WPI Advanced Institute for Materials Research, Tohoku University, 2–1–1 Katahira, Aoba-ku, Sendai 980–8577, Japan
[15]Design and Producing Field, Corrosion Resistant Alloy Group, Research Center for Structural Materials, NIMS, 1–2–1 Sengen, Tsukuba, Ibaraki 305–0047, Japan
[16]Kyoto University Institute for Advanced Study, Kyoto University, Yoshida Ushinomiya-cho, Sakyo-ku, Kyoto 606–8501, Japan
[17]Center for Advanced Intelligence Project, RIKEN, 1–4–1 Nihonbashi, Chuo-ku, Tokyo 103–0027, Japan
[18]National Institute of Technology, Hakodate College, 14–1 Tokura-cho, Hakodate, Hokkaido 042–0953, Japan

The structure of glassy, liquid, and amorphous materials is still not well understood, due to the insufficient structural information from diffraction data. In this article, attempts are made to understand the origin of diffraction peaks, particularly of the first sharp diffraction peak (FSDP, Q_1), the principal peak (PP, Q_2), and the third peak (Q_3), observed in the measured diffraction patterns of disordered materials whose structure contains tetrahedral motifs. It is confirmed that the FSDP (Q_1) is not a signature of the formation of a network, because an FSDP is observed in tetrahedral molecular liquids. It is found that the PP (Q_2) reflects orientational correlations of tetrahedra. Q_3, that can be observed in all disordered materials, even in common liquid metals, stems from simple pair correlations. Moreover, information on the topology of disordered materials was revealed by utilizing persistent homology analyses. The persistence diagram of silica (SiO_2) glass suggests that the shape of rings in the glass is similar not only to those in the crystalline phase with comparable density (α-cristobalite), but also to rings present in crystalline phases with higher density (α-quartz and coesite); this is thought to be the signature of disorder. Furthermore, we have succeeded in revealing the differences, in terms of persistent homology, between tetrahedral networks and tetrahedral molecular liquids, and the difference/similarity between liquid and amorphous (glassy) states. Our series of analyses demonstrated that a combination of diffraction data and persistent homology analyses is a useful tool for allowing us to uncover structural features hidden in halo pattern of disordered materials.

Key-words : Glass, Liquid, Amorphous materials, Structure, X-ray diffraction, Neutron diffraction, Topology, Persistent homology

† Corresponding author: S. Kohara; E-mail: KOHARA.Shinji@nims.go.jp

[Received July 8, 2019; Accepted October 4, 2019]

1. Introduction

The absence of translational symmetry, and the very much present complexity in the structure of glassy, liquid, and amorphous materials make glass science a challenging field. Indeed, as noted by Egelstaff in his review article in 1983,[1] solving the structure of disordered materials can be frustrating: although the underlying concepts have been known for a while, appropriate measurement methods for high-quality diffraction data are often not available. However, the advance of instrumentation and measurement protocols makes it feasible to use X-ray diffraction (XRD) and neutron diffraction (ND) techniques to investigate the structure of disordered materials at synchrotron and neutron facilities.[2] Moreover, a combination of diffraction experiments and advanced computer simulation techniques enables understanding of the structure of disordered materials at both the atomistic and electronic levels.[3]

In ND and XRD measurements on disordered materials containing n chemical species, structural information is contained in the total structure factor[2),3)]

$$S(Q) = 1 + \frac{1}{|\langle W(Q)\rangle|^2}\sum_{i=1}^{n}\sum_{j=1}^{n} c_i c_j w_i^*(Q) w_j(Q)\big[S_{ij}(Q) - 1\big] \quad (1)$$

where c_i is the atomic fraction of chemical species i; $w_i(Q)$ is either a Q-independent coherent scattering length in ND or a Q-dependent atomic form factor with dispersion terms in XRD and is, in general, a complex number; $S_{ij}(Q)$ is the partial structure factor. $|\langle W(Q)\rangle|^2 = \sum_{i=1}^{n}\sum_{j=1}^{n} c_i c_j w_i^*(Q) w_j(Q)$. The corresponding real space information is contained in the total correlation function $T(r)$, which is obtained by the Fourier transform relation

$$T(r) = 4\pi r\rho + \frac{2}{\pi}\int_{Q_{\min}}^{Q_{\max}} Q\big[S(Q) - 1\big]\sin(Qr)dQ \quad (2)$$

where r is a distance in real space and ρ is the atomic number density. By using real space function, it is possible to obtain inter-atomic distances and coordination numbers.[2),3)]

Typical glass-forming materials, e.g., glassy (g-) silica (SiO_2), $GeSe_2$, and $ZnCl_2$, have a network structure, in which atoms are connected with (at least partially) covalent bonds. For instance, the short-range structure in g-SiO_2 is a SiO_4 tetrahedron, and the interconnection of tetrahedra form a network with sharing oxygen atoms at the corner. This polyhedral motif is manifested by a first sharp diffraction peak (FSDP) and a principal peak (PP) in structure factor $S(Q)$.[4] The FSDP was first discussed in 1976,[5] although it appears that the name "FSDP" was first used by Phillips in 1981.[6] The interpretation of diffraction peaks including the FSDP was attempted in the 1980s[6),7)] and details are discussed in several papers.[8)–11)] It is known that the FSDP of silica glass is related to the formation of the random network model of Zachariasen[12] and the model was extended to silicate glass as illustrated in Fig. 7 of Ref. 11 by Mei et al. It was confirmed that intermediate-range ordering arises from the periodicity of boundaries between successive small cages in the network formed by connected, regular SiO_4 tetrahedra with shared oxygen atoms at the corners associated with the formation of a ring structure and a cavity.[13] The second maximum, the PP, reflects the size of the local-network-forming motif, whereas the FSDP indicates the arrangement of these motifs on an intermediate range according to Zeidler and Salmon.[14] Another interpretation of the FSDP was recently proposed by Shi and Tanaka, who discussed local tetrahedral ordering in covalent liquids and glasses.[15]

Recent progress in simulation techniques, coupled with the development of atomic configuration analysis tools, has allowed us to study structural order beyond the first correlation sphere.[2),3)] In particular, topological analysis tools to investigate the distribution of rings[16] and cavities[17] are important for understanding atomic ordering in disordered materials.

Another important structural descriptor in this article is homology.[18] Recently, topological data analysis has rapidly progressed and has provided several tools for analyzing multiscale data in physical and biological fields.[18] Hiraoka et al. applied persistent homology to disordered materials to understand the homology of rings, which cannot be detected by conventional ring statistics analysis,[18] following the landmark study of Hirata et al.[19] This mathematical tool, based on the persistence diagram (PD), was developed to capture shapes of multiscale data. The input to the PDs is given by atomic configurations and the output is expressed as 2D histograms. Then, specific distributions such as curves and islands in the PDs identify meaningful shape characteristics of the given atomic configuration.

In this article, we try to unravel the structural origin of diffraction patterns from several disordered materials with tetrahedral motifs to understand the nature of order within disorder.[20] Although most of diffraction data are taken from the literature, we performed additional diffraction measurements on g-$Cu_{50}Zr_{50}$ and liquid (l)-Si, because the former is a reference, whose atomic structure is very far away from tetrahedral motif due to the lack of chemical bond and the latter is important to understand the structural difference between a-Si and l-Si. We also performed several reverse Monte Carlo (RMC)[21] and/or molecular dynamics (MD) simulations for liquid and glassy Si and SiO_2. To understand the origin of Q_3, RMC modeling on l-Hg was conducted. Furthermore, persistent homology analysis was applied to structural models to reveal the relationship between diffraction patterns and topology/homology.

2. Experimental and simulation procedures

$Cu_{50}Zr_{50}$ glass ribbons (g-$Cu_{50}Zr_{50}$) were prepared by the melt-spun method. The master alloy was prepared by arc melting in an argon atmosphere. Ribbon samples with a cross section of 1 mm × 0.03 mm were fabricated from

the master alloy in a single-roll melt spinner. High-energy XRD experiments on the glass were conducted at the BL04B2[22] and BL15XU beamlines at the SPring-8 synchrotron radiation facility. The energies of the incident X-rays were 61.4 keV (BL04B2) and 30.0 keV (BL15XU).

Containerless high-energy XRD measurements were performed on liquid silicon (*l*-Si) using an aerodynamic levitation technique at an incident energy of 113 keV at the BL04B2 beamline. A sample was processed by conical nozzle levitation using filter-purified Ar gas (impurity <0.01 mass ppm). A 200 W CO_2 laser was used to heat the sample and the temperature was measured using a two-color pyrometer. The measured diffraction data were corrected for polarization, absorption, and the background, and the contribution of Compton scattering was subtracted using standard data analysis software.[23] Fully corrected data were normalized to give the Faber–Ziman[24] total structure factor $S(Q)$.

MD simulation for *g*-SiO_2 was performed using the large-scale atomic/molecular massively parallel simulator (LAMMPS) package[25] employing Born–Mayer-type pair correlations. As the initial atomic configuration, 3000 atoms (Si, 1000; O, 2000) were randomly distributed in a cubic cell with respect to the experimental density. The simulation was performed with a time step of 1 fs in the NVT ensemble. The simulation temperature was maintained at 4000 K for 20,000 time steps, then the temperature was reduced to 300 K over 200,000 time steps. Finally, the system was equilibrated at 300 K for 50,000 time steps. A Nosé–Hoover thermostat was employed to control the temperature. After the MD simulation, the obtained configuration was refined by RMC simulations with constraints on the coordination number and the O–Si–O bond angle distribution, to prevent the formation of an unfavorable disordered structure. The RMC++ code was used.[26]

The RMC model for *l*-Hg (5000 particles) was obtained using the RMC++ code, on the basis of the X-ray pair distribution function $g^{X}(r)$[23] up to 4 Å (1 Å = 0.1 nm) (first inter-atomic distance). The RMC models for *l*-Si (1770 K, 5000 particles), the low-pressure molecular *l*-P (0.96 GPa/1328 K, 5000 particles), and the high-pressure network *l*-P (1.01 GPa/1323 K, 5000 particles) were obtained using the RMC++ code with the X-ray $S(Q)$ for *l*-Si and *l*-P,[27] starting from random configurations. The formation of P_4 tetrahedra and three-fold phosphorous were constrained for low-pressure and high-pressure *l*-P, respectively.

The model for *a*-Si was generated by a melt quenching procedure using MD simulation, followed by RMC refinement, using the experimental X-ray $S(Q)$.[28] The MD simulation was implemented using the LAMMPS code. The simulation box was a cube with a side length of 50 Å. It had a number density of about 0.050 $Å^{-3}$, which is consistent with a bulk density of 2.33 g cm^{-3}. In the simulation, 6256 Si atoms were generated within the NVT ensemble. A time step of 1 fs was used in the Verlet algorithm. The interactions were described by a bond-order-type interatomic potential[29] based on the three-body Tersoff potential.[30),31] The atomic configuration was initialized at random and then the system was equilibrated at 3000 K for 500,000 steps. Then it was cooled to 300 K during for 5,000,000 steps and annealed at 300 K for 500,000 steps. The atomic configuration generated by the MD simulation was refined using the RMC++ code, so that the model reproduces the experimental X-ray $S(Q)$.

The homology of atomic configurations was investigated by the PD obtained using the HomCloud package.[33] Given a set of points in the space, the persistent homology captures its topological multiscale structures, and those identified structures are compactly expressed in the PD. The construction of the PD follows the process schematically depicted in **Fig. 1**(A). We first replace each point with a sphere and increase the radius from zero to sufficiently large value, which corresponds to the changing resolution of input x, y, z coordinates of atoms. Then, we record the pair of radii (b, d) at which a ring in a specific location appears (birth) and disappears (death), respectively. The PD is a histogram of the birth/death plane counting of rings at the coordinate (b, d). From this construction, it enables one not only to count the number of rings, but also to characterize their shapes at multiscale. Typical examples of birth/death pairs for typical regular structures were shown in Figs. 1(B)–1(D). For regular hexagonal points whose distance between points is a, the ring appears at radius $a/2$ and disappears at radius a, as shown in Fig. 1(B). For a regular triangular configuration, the ring appears at $a/2$ and disappears at $\sqrt{1/3}a \approx 0.577a$, as shown in Fig. 1(C), and the one-dimensional PD for regular hexagonal/triangular points is shown in Fig. 1(D). In this paper, PDs are being used for investigating rings and polyhedral formations in atomic configurations. We also note that the detected rings are recorded during the computation of the diagrams, and hence we can explicitly identify their geometric shapes.

3. Results and discussion

Figure 2 shows total structure factors, $S(Q)$, for amorphous (*a*)-Si,[28] glassy (*g*)-$ZnCl_2$,[34] *g*-$GeSe_2$,[35] *g*-GeS_2,[36] *g*-GeO_2,[37] *g*-SiO_2,[38] *l*-CCl_4,[39] and *l*-P[27] obtained by ND and XRD. The short-range structural unit of these materials is a tetrahedron, although all amorphous and glassy materials form a network whereas the two liquids are molecular liquids in which CCl_4 and P_4 tetrahedra are isolated. In the figure, a three-peak structure,[14] Q_1 (FSDP), Q_2 (PP), and Q_3, can be observed in the $S(Q)$ when the scattering vector Q is scaled by multiplying by the distance between the center and corner of a tetrahedron in all glassy materials except *a*-Si, although a four-peak structure is found in molecular liquids due to the split of Q_2. Both *g*-$ZnCl_2$[34] and *g*-$GeSe_2$[35] make a small contribution to the edge sharing of tetrahedra in addition to corner sharing, but it is presumable that the three-peak structure arises from mainly corner-sharing tetrahedral motifs, because the contribution of edge sharing is very small in comparison with corner-sharing.[34),35] The FSDP of *g*-GeO_2 has a

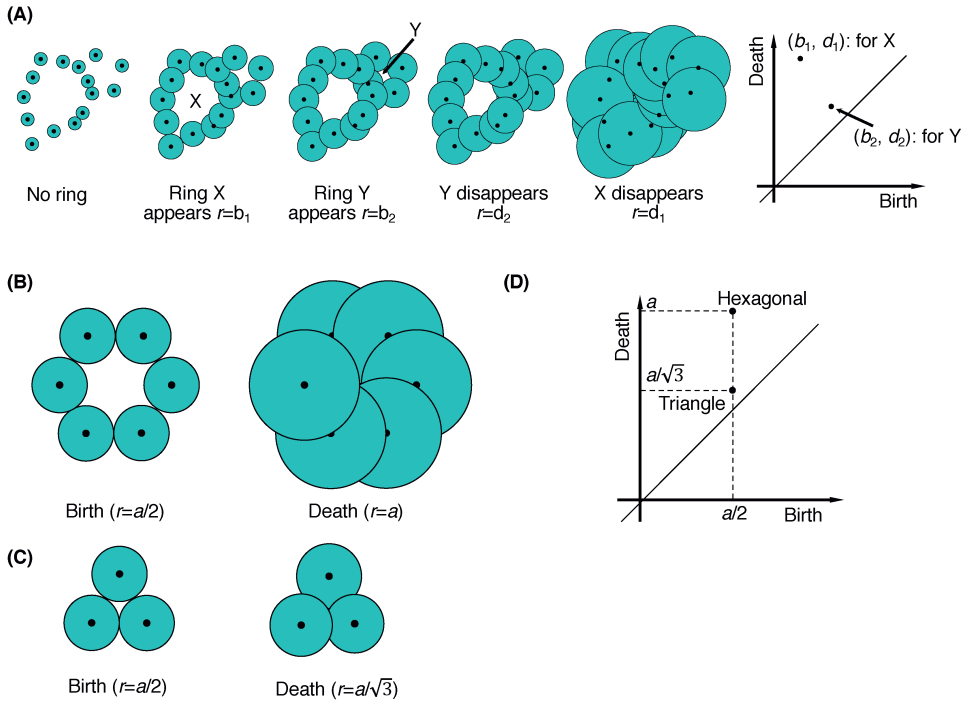

Fig. 1. Persistent homology and PD. (A) The increasing sequence of spheres for input data (left). The PD (right) is obtained as a histogram counting the number of rings on the birth-death plane. (B), (C) The appearance and disappearance of a ring for a regular hexagon/triangle. (D) The pairs of birth and death radii for hexagon and triangle in the one-dimensional PD.

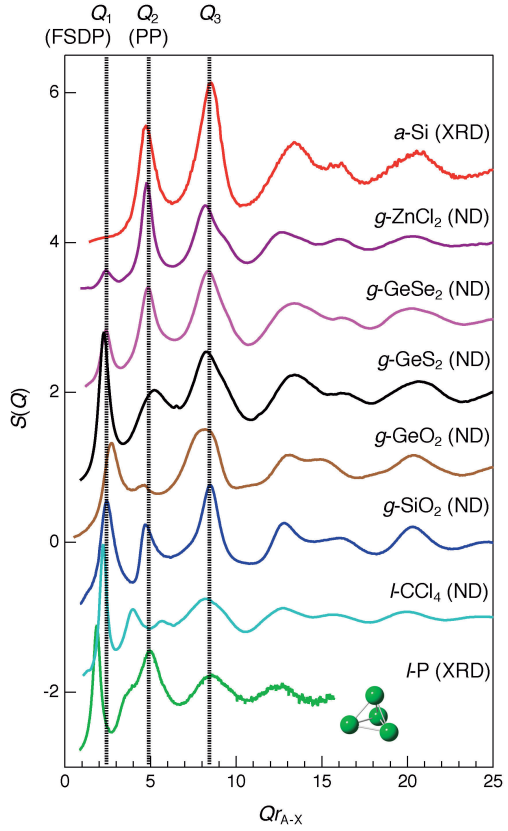

Fig. 2. Total structure factors, $S(Q)$, for a-Si,[28] g-$ZnCl_2$,[34] g-$GeSe_2$,[35] g-GeS_2,[36] g-GeO_2,[37] g-SiO_2,[38] l-CCl_4,[39] and l-P.[27] The scattering vector Q is scaled by multiplying by $r_{A\text{-}X}$ (distance between center and corner of tetrahedra. In the case of l-P, $r_{A\text{-}X}$ is estimated from the side length of P_4 tetrahedron.

larger $Qr_{A\text{-}X}$ value, implying that this behavior is related to the higher oxygen packing fraction in g-GeO_2[40),41)] than that in g-SiO_2. The FSDP is, however, also observed in the $S(Q)$ of l-CCl_4,[8)] l-KPb,[42)–44)] l-P (see Fig. 2) and other molecular liquids,[45)] confirming that the FSDP is not a signature of the formation of a polyhedral network. Indeed, an FSDP has been observed in many other network formers, such as g-B_2O_3[46)] and g-As_2O_3,[47)] but not in a-Si, a-Se, g-$Pd_{42.5}Ni_{7.5}Cu_{30}P_{20}$,[14)] or l-Hg,[23)] although Shi and Tanaka recently pointed out that a-Si shows an FSDP.[15)] Therefore, we show that the FSDP is the signature of the successive polyhedra with the periodicity given by $2\pi/Q_{FSDP}$ as illustrated in **Fig. 3**. It is possible to recognize a periodicity of ~4 Å (indicated by blue arrows) with a correlation length of ~10 Å (indicated by magenta arrows), which is in line with Gaskell and Wallis's estimation.[48)] That is, the FSDP appears as the result of a sparse distribution of planes in polyhedra, because the FSDPs of g-SiO_2[32),49)] and l-P[27)] diminish with increasing pressure associated with the reduction of cavities.

Since the origin of the FSDP has been discussed for a long time, as mentioned above, we calculated the periodicity and correlation length given by $2\pi/Q_{FSDP}$ and $2\pi/\Delta Q_{FSDP}$, respectively, by a Lorentzian peak fit to the FSDPs, as summarized in **Table 1**. Although several discrepancies with a previous report[10)] are observed, the overall trends remain almost the same. It is found that chalcogenide glasses exhibit very long correlation lengths, and the correlation lengths of l-CCl_4 and l-P are longer than those of AX_2 oxide glasses. This behavior implies

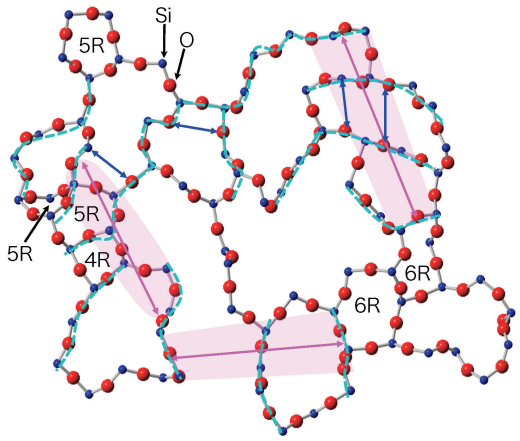

Fig. 3. RMC-MD-generated atomic configuration for g-SiO_2. The thickness of the cell is approximately 9 Å and only the atoms belonging to the network are shown.

Table 1. FSDP parameters obtained from the neutron $S(Q)$ data for a series of disordered materials. Typical errors in Q_{FSDP} are ± 0.02 Å^{-1}

Sample	Position Q_{FSDP} (Å^{-1})	FWHM ΔQ_{FSDP} (Å^{-1})	Periodicity $2\pi/Q_{FSDP}$ (Å)	Correlation length $2\pi/\Delta Q_{FSDP}$ (Å)
g-$ZnCl_2$	1.06	0.65	5.91	9.74
g-$GeSe_2$	1.01	0.33	6.21	18.93
g-GeS_2	1.04	0.31	6.06	20.59
g-GeO_2	1.58	0.65	3.99	9.71
g-SiO_2	1.51	0.64	4.15	9.90
l-CCl_4	1.28	0.34	4.91	18.48
l-P	1.37	0.45	4.59	13.89

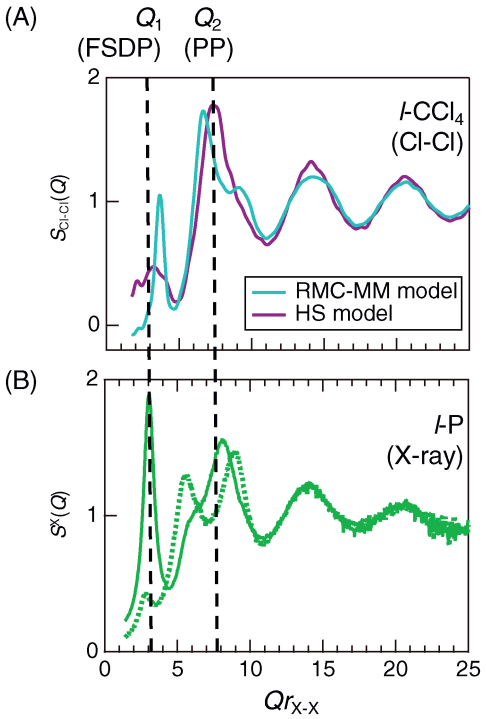

Fig. 4. (A) RMC-MM generated Faber–Ziman partial structure factor, $S_{Cl-Cl}(Q)$, for l-CCl_4,[39] together with that of the reference HS model. (B) X-ray $S(Q)$ for l-P[27] measured at 0.96 GPa/1328 K (low-density molecular liquid, solid green curve) and 1.01 GPa/1323 K (high-density network liquid, dotted green curve). The scattering vector Q in all data sets was scaled by r_{X-X} (distance between the corners of tetrahedra).

that the tetrahedra in these materials have much more freedom in their orientational arrangements for ordering than those in oxide glasses with relatively stronger covalent bonds. To shed light on the long correlation length, we compare the partial structure factors of Cl–Cl, $S_{Cl-Cl}(Q)$, for l-CCl_4 obtained by RMC-molecular mechanics (MM) modeling[39] with the $S_{P-P}(Q)$ (experimental XRD data) for l-P (solid green curve, molecular liquid; dotted green curve, network liquid),[27] as shown in **Fig. 4**, where the scattering vector Q is scaled by the side length of the tetrahedra. In the case of l-CCl_4, we calculated $S_{Cl-Cl}(Q)$ for both the final RMC model and the hard sphere Monte Carlo (HS) model (RMC modeling without experimental data) as a reference [solid purple curve in Fig. 4(A)]. In the case of oxide glass, the origin of the PP is clearly visible in the neutron $S(Q)$ of g-SiO_2 under high pressures,[49] in which the PP reflects the packing of oxygen atoms (at corners of tetrahedra).[50] The PP observed in the $S_{Cl-Cl}(Q)$ of the HS model for l-CCl_4 (random distribution of CCl_4 molecules) shown as a purple curve, is a singlet. However, the experimental data for l-CCl_4 shown in Fig. 2 exhibits a doublet peak, which is a signature of the formation of orientational correlations of CCl_4 tetrahedra as suggested by Misawa[51] and Pothoczki et al.,[45),52] and it is reproduced in the RMC-MM model shown as a solid cyan curve in Fig. 4(A). The details of the orientational correlation in the liquid are discussed in Ref. 45. This behavior implies that distinct orientational correlations are formed in l-P [see Fig. 4(B)] and probably in g-As_2O_3[47] because they have a doublet PP in the $S(Q)$. Thus, the PP seems to reflect inter-polyhedral correlations in disordered materials, yielding a shorter-length scale in comparison with FSDP. It should be stressed that the transform from a molecular liquid [low-density form, solid green curve in Fig. 4(B)] to a network liquid [high-density form, dotted green curve in Fig. 4(B)] in l-P under high pressures and high temperatures results in a diminished FSDP, even though the high-pressure liquid forms a network. The prominent FSDP appearing in the experimental X-ray $S(Q)$ of the low-density molecular l-P [shown as a solid green curve in Fig. 4(B)] as well as the $S_{Cl-Cl}(Q)$ of the RMC-MM model for l-CCl_4 [shown as a solid cyan curve in Fig. 4(A)] suggests that the FSDP appears without the center atom of tetrahedron, because the FSDP of l-P is prominent even though a P_4 tetrahedron does not have a central atom of tetrahedron.

The third peak Q_3 of the three-peak structure has not yet been discussed in depth to the best of our knowledge, because it presumably reflects the succession of single-pairwise correlations, while Q_1 and Q_2 reflect the succession of multi-pairwise correlations, and hence might be observed in all amorphous materials. The X-ray structure

factor, $S^X(Q)$, for l-Hg[23] is shown in **Fig. 5**, together with the result of RMC modeling. The $S(Q)$ calculated from the RMC model, generated by fitting only the experimental $g(r)$ up to 4 Å, reproduces Q_3 very well, implying that Q_3 reflects the formation of pairwise correlations (note that this confirmation is valid only in a dense random packing structure[53] such as that in the single-element liquids in our study).

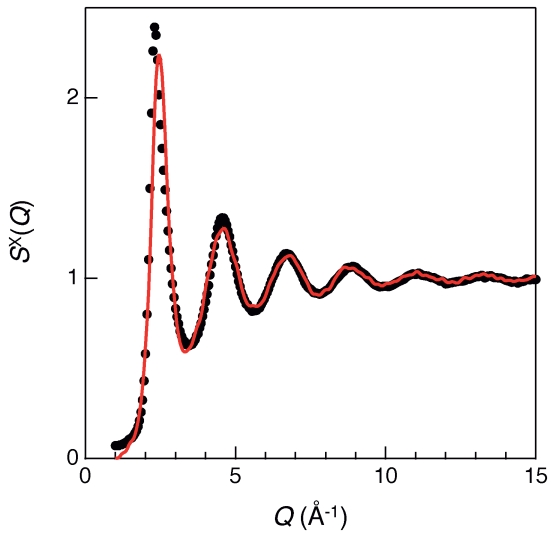

Fig. 5. X-ray structure factor, $S^X(Q)$, for l-Hg[23] together with the result of RMC modeling using X-ray pair distribution function $g^X(r)$ up to 4.0 Å. Black circles, experimental data; red curve, RMC model.

The X-ray and neutron[54] total structure factors, $S(Q)$, of g-$Cu_{50}Zr_{50}$ are shown in **Fig. 6**(A) together with the X-ray $S(Q)$ for a-Si,[28] and neutron $S(Q)$ for g-SiO_2[38] and l-CCl_4.[39] The scattering vector Q in the figure is scaled by multiplying by d [first inter-atomic distance appearing in the real-space function obtained by Fourier transform of $S(Q)$], because the short-range structural unit is not a tetrahedron in g-$Cu_{50}Zr_{50}$.[54] It is worth mentioning that the g-$Cu_{50}Zr_{50}$ metallic glass does not have a distinct FSDP or PP, which is consistent with the neutron $S(Q)$ for g-$Cu_{50}Zr_{50}$ obtained with the isotopic substitution technique.[55] Figures 6(B) and 6(C) show the $S(Q)$ for a-Si[28] and g-SiO_2[38] with different length scaling of Q. The scaling with $r_{A\text{-}X}$ shown in Fig. 6(B) suggested by Elliott,[8] Wright,[9] Benmore et al.,[56] and Zeidler and Salmon,[14] demonstrates that a-Si does not exhibit an FSDP. On the other hand, the scaling by $r_{A\text{-}A}$ (scaled by Si–Si interatomic distance) recently proposed by Shi and Tanaka[15] shown in Fig. 6(C) gives rise to an FSDP for both g-SiO_2 and a-Si.

The pairwise correlation function is an adequate descriptor of disordered materials since we can apply it for cases with or without a Bragg peak in reciprocal-space data; hence, the pair distribution function $g(r)$ has been widely applied to glassy, liquid, and amorphous materials. However, atomistic ordering beyond the first correlation

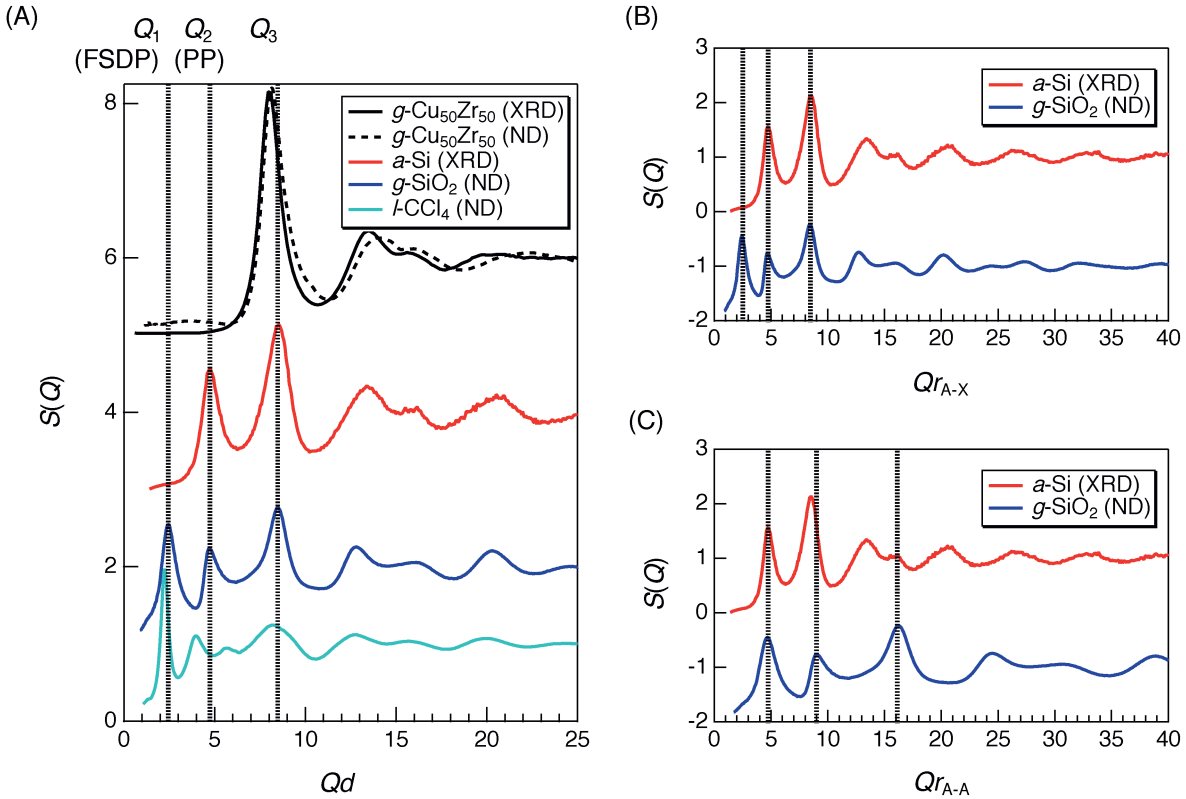

Fig. 6. (A) Total structure factors, $S(Q)$, for g-$Cu_{50}Zr_{50}$ (XRD), g-$Cu_{50}Zr_{50}$ (ND),[54] a-Si,[28] g-SiO_2,[38] l-CCl_4,[39] (B) $S(Q)$ for a-Si,[28] g-SiO_2[38] scaled by $r_{A\text{-}X}$ (distance between center and corner of tetrahedra), (C) $S(Q)$ for a-Si,[28] g-SiO_2[38] scaled by $r_{A\text{-}A}$ (distance between the centers of tetrahedra). A small prepeak is observed at $Qd \sim 3.5$ in the neutron $S(Q)$ for g-$Cu_{50}Zr_{50}$ stems from the formation of subtle chemical ordering.[2]

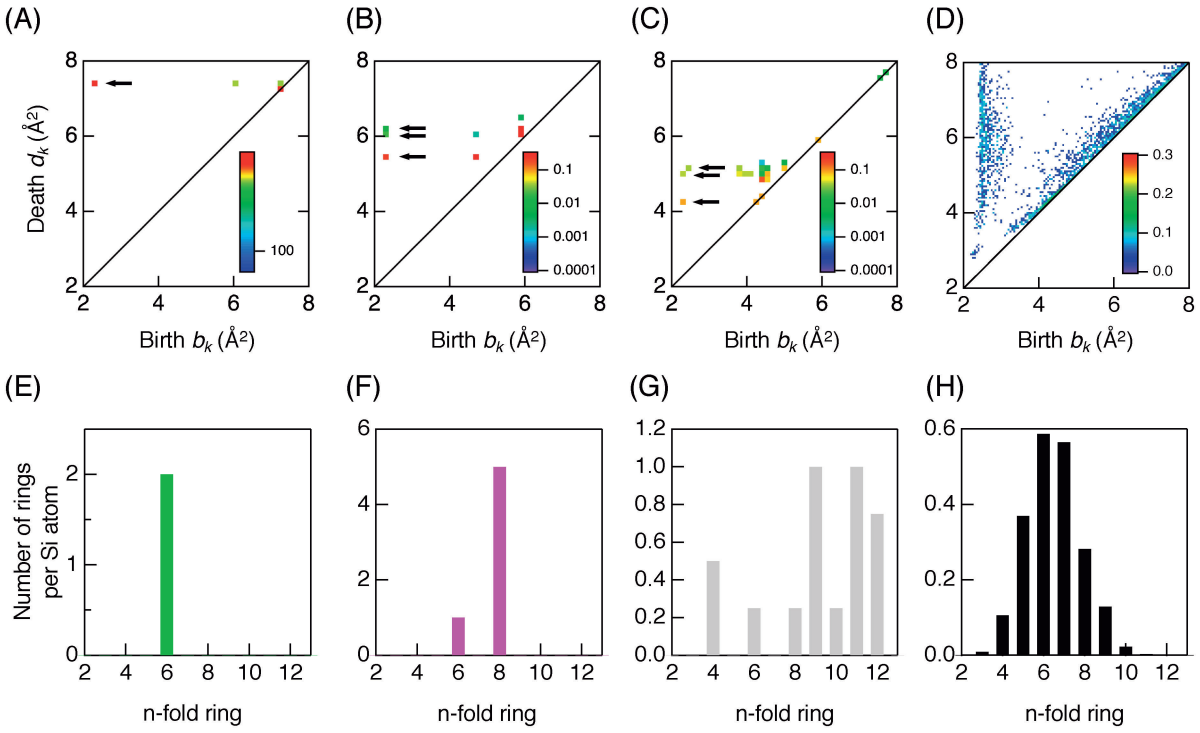

Fig. 7. Si-centric PDs for (A) α-cristobalite, (B) α-quartz, (C) coesite, and (D) g-SiO_2. Primitive ring statistics for (E) α-cristobalite, (F) α-quartz, (G) coesite, and (H) g-SiO_2.

sphere has recently been determined by advanced simulation and topological analyses.[2),3)] In particular, since persistent homology analysis was first applied to the topological analysis of a bulk metallic glass in 2013,[19)] two landmark studies have been reported.[18),32)] We therefore now turn to detailed persistent homology analyses of structural models of materials mentioned in this article. **Figures 7**(A)–7(D) show the Si-centric PDs calculated from the crystal structures for α-cristobalite ($d = 2.327$ g cm^{-3}),[57)] α-quartz ($d = 2.655$ g cm^{-3}),[58)] and coesite ($d = 2.905$ g cm^{-3}),[59)] together with that of g-SiO_2 ($d = 2.2$ g cm^{-3}) obtained from RMC-MD modeling. The primitive ring statistics of silica crystals and the glass are shown in Figs. 7(E)–7(H). α-cristobalite shows only sixfold rings consisting of six SiO_4 tetrahedra, while α-quartz has a large fraction of eightfold rings in addition to sixfold rings. On the other hand, both coesite and g-SiO_2 exhibit a distribution of different size rings, which is a sign of topological disorder according to Gupta and Cooper.[60)] A systematic change in the Si-centric PDs with density is observed for the crystalline phases in Figs. 7(A)–7(C). In contrast to the crystalline phases, the PD for g-SiO_2 has a vertical profile along the death axis at $b_k \sim 2.2$ Å^2, which is thought to be a signature of the formation of a –Si–O–Si–O– glass network.[18)] The comparison between Si-centric PDs and primitive ring size distributions shown in Fig. 7 provides us with comprehensive topological information, because ring size distribution analysis is sensitive to the ring size, whereas PDs make it possible to reveal the shape of rings. Since all forms of silica have corner-sharing SiO_4 tetrahedral motifs, a comparison of α-cristobalite, α-quartz, and coesite with g-SiO_2 in the Si-centric PDs suggests that the glass has not only the homology of a crystalline phase with comparable density (α-cristobalite), but also the homology of higher-density crystalline phases (α-quartz and coesite). It is known that g-SiO_2 has a distribution of ring size [topological disorder,[60)] see Fig. 7(H)],[61),62)] but Figs. 7(E)–7(G) indicate that crystalline phases exhibit topological disorder with increasing density, because ring size distributions become broad with increasing density. It is concluded from a combination of PD analysis and conventional ring statistical analysis that the vertical profile along the death axis observed in the Si-centric PD for g-SiO_2 is the result of disorder, because the small death value in the glass implies that the arrangement of SiO_4 tetrahedra is locally more densely packed in the glass than in α-cristobalite, whose density is comparable to g-SiO_2.

The Si-centric/O-centric PDs for g-SiO_2 and the C-centric/Cl-centric PDs for l-CCl_4 are compared in **Figs. 8**(A) and 8(B) (left and center panels), respectively. As mentioned above, a vertical profile along the death axis at $b_k \sim 2.2$ Å^2 is observed in the Si-centric PD for g-SiO_2, whereas no such profile is observed in the C-centric PD for l-CCl_4. A vertical profile is observed in the O-centric PD, too. In addition, the FSDP in l-CCl_4 is much narrower than that in g-SiO_2, as shown in Figs. 8(A) and 8(B) (right panels). This behavior demonstrates that the correlation length in the former is longer than that in the latter (see Table 1). However, the C-centric PD for l-CCl_4 does not have a well-defined profile, whereas a vertical profile along the death axis is observed in the Si-centric PD for g-SiO_2, indicating the formation of a tetrahedral network

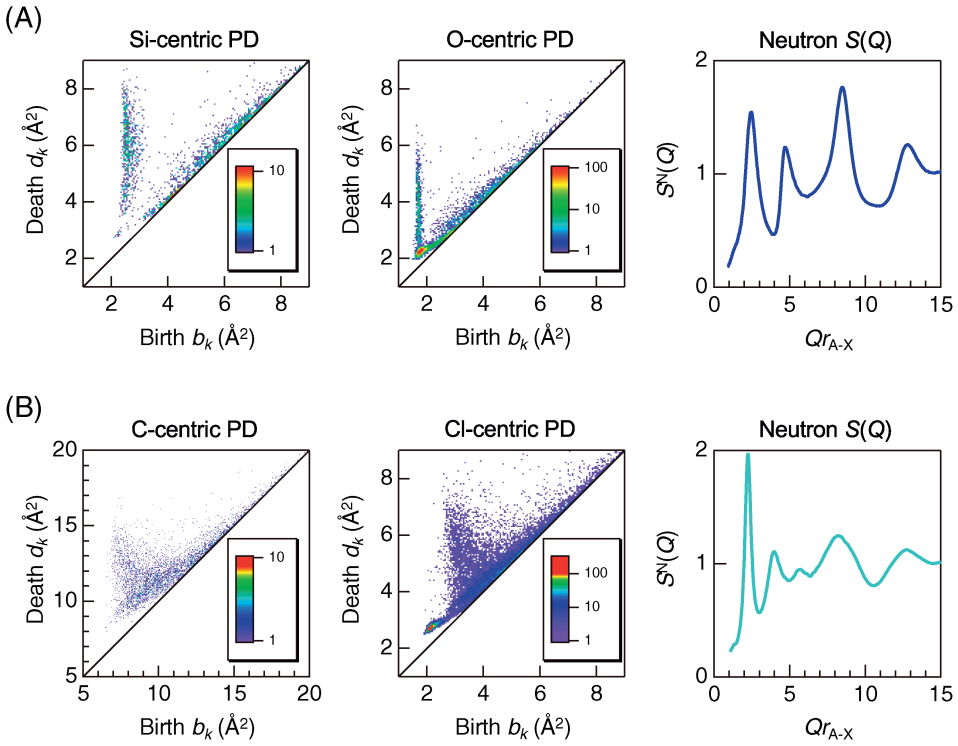

Fig. 8. (A) Si-centric PD, O-centric PD, and neutron $S(Q)$ for g-SiO_2.[38] (B) C-centric PD, Cl-centric PD, and neutron $S(Q)$ for l-CCl_4.[39]

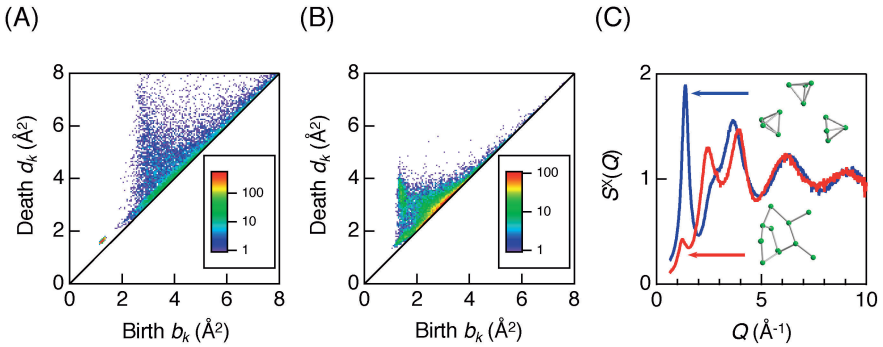

Fig. 9. P-centric PDs for l-P at (A) 0.96 GPa/1328 K (low-density molecular liquid) and at (B) 1.01 GPa/1323 K (high-density network liquid). (C) X-ray $S(Q)$ for l-P at 0.96 GPa/1328 K (blue curve, low-density molecular liquid) and 1.01 GPa/1323 K (red curve, high-density network liquid).[27]

in the glass. Moreover, the Cl-centric PD for l-CCl_4 does not exhibit a vertical profile, suggesting the absence of a network in the liquid, although the FSDP is sharp. Similar behavior is observed in l-P under high pressures and high temperatures. **Figures 9**(A) and 9(B) show the PDs for l-P.[27] The profile of molecular liquid shown in Fig. 9(A) is very similar to that of l-CCl_4 shown in Fig. 8(B), because l-CCl_4 is a molecular liquid, in which there is no network formation. On the other hand, the network liquid exhibits a vertical profile [Fig. 9(B)], indicating the formation of a –P–P–P– network. This difference can be clearly observed in the X-ray $S(Q)$ shown in Fig. 9(C), where it is possible to observe an FSDP for the molecular liquid (blue curve), which diminishes in the network liquid (red curve). Thus, on the basis of both PD analysis and diffraction data, we can reasonably conclude that the FSDP is not a signature of the formation of a network.

The structural difference between liquid and glass (amorphous) is an important topic for understanding the nature of glass and glass formation. We tackle this issue by focusing on Si and SiO_2, which was also highlighted in a recent article by Shi and Tanaka.[15] First of all, it is necessary to ensure differences in the short-range structure and density, because the former is a very important parameter for discussing the structure, and the latter is necessary for performing MD and/or RMC simulations. The Si–O coordination numbers N_{Si-O} is approximately 4.0 in g-SiO_2 and 3.9 in l-SiO_2. These values are consistent with the results of the MD simulation reported by Takada et al.[63] The density of g-SiO_2 is 2.2 g cm^{-3} and that of l-SiO_2 is 2.1 g cm^{-3}

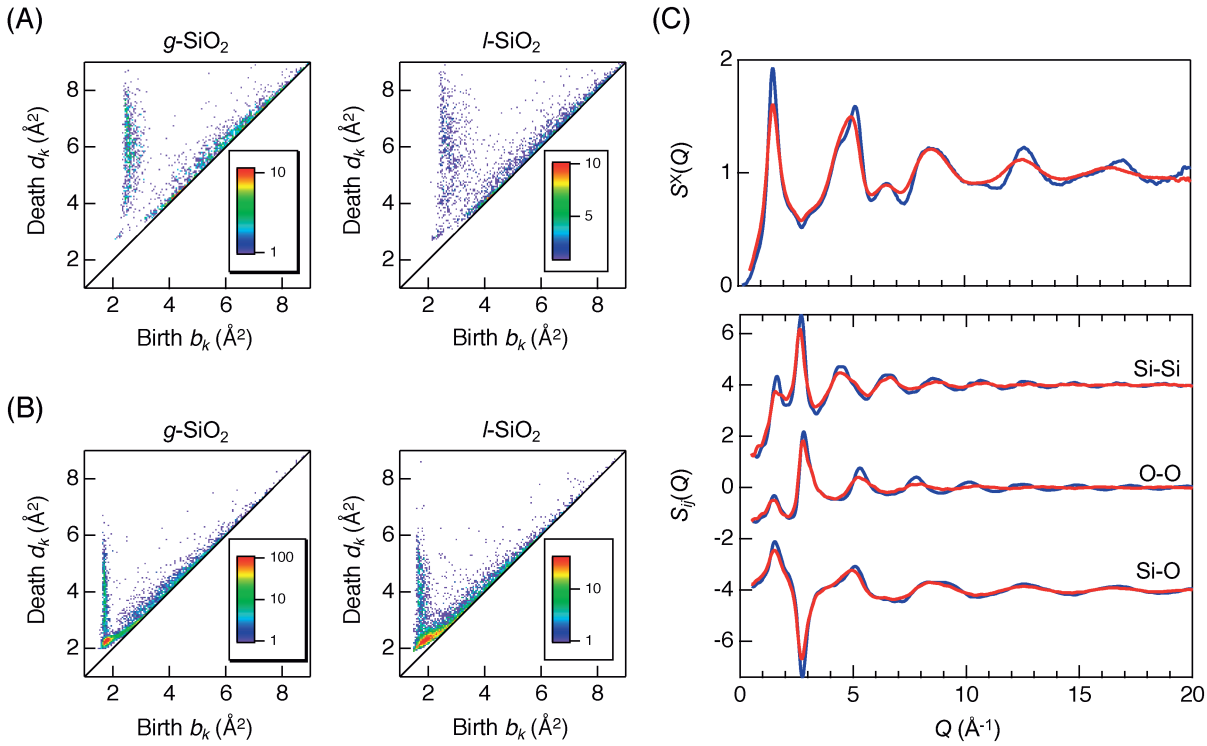

Fig. 10. (A) Si-centric PD for g-SiO_2 and l-SiO_2. (B) O-centric PD for g-SiO_2 and l-SiO_2. (C) X-ray total structure factors (upper), $S^X(Q)$, for g-SiO_2[38] and l-SiO_2 (2323 K)[64] together with the RMC-MD-generated partial structure factors (lower), $S_{ij}(Q)$, for g-SiO_2 (blue curves) and l-SiO_2 (red curves, 2323 K).

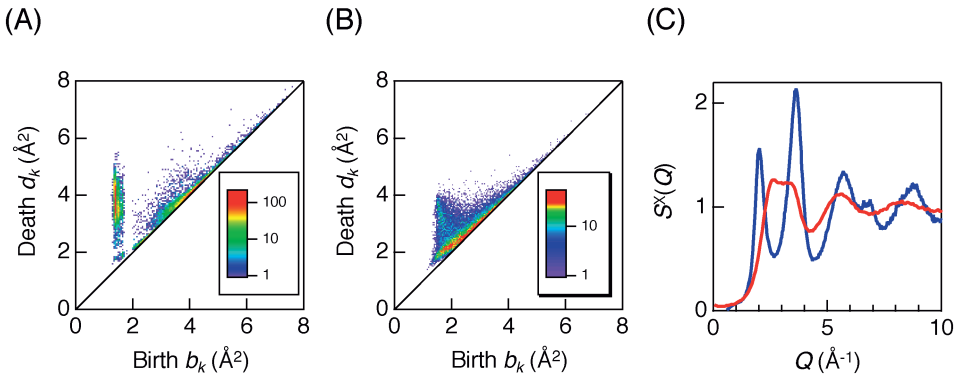

Fig. 11. Si-centric PDs for (A) a-Si and (B) l-Si (1770 K). (C) X-ray $S(Q)$ for a-Si (blue curve)[27] and (B) l-Si (red curve, 1770 K).

(2373 K),[64] resulting in a small difference between the glassy and liquid phases. In the case of silicon, the coordination number is 4.0 in the amorphous phase and 5.7 in the liquid phase, and the density of the former is 2.3 g cm^{-3},[28] whereas that of the latter is 2.57 g cm^{-3} (1770 K).[65] There are significant differences in the coordination number and density between two phases in Si owing to the fact that the amorphous phase is a semiconductor and the liquid phase is metallic.

Figures 10(A) and 10(B) show the Si-centric and O-centric PDs for g-SiO_2 and l-SiO_2 (2373 K). Both the glassy and liquid data exhibit a vertical profile along the death axis. The experimental $S^X(Q)$ (upper) and RMC-MD-generated Faber–Ziman partial structure factors, $S_{ij}(Q)$ (lower), for g-SiO_2 (blue curves) and l-SiO_2 (red curves) are shown in Fig. 10(C). Although the peaks are broader in the liquid, it appears that the FSDP is still dominant in the liquid. Both the Si-centric PDs shown in Figs. 10(A) and 10(B), and the X-ray $S(Q)$ (top) and the partial structure factors, $S_{ij}(Q)$ (bottom), in Fig. 10(C) show only little differences between the glassy and liquid phases, suggesting that the Si–O network is very massive even in the liquid phase. This feature can be reasonably understood from the very high viscosity of l-SiO_2,[66] and hence it is consistent with the concept of a "strong liquid" proposed by Angell.[67]

The Si-centric PDs for a-Si and l-Si (1770 K) are depicted in **Figs. 11**(A) and 11(B), respectively. The profiles are

not identical and this behavior shows sharp contrast with the SiO_2 case shown in Figs. 10(A) and 10(B), because the coordination number in *a*-Si is approximately 4 whereas that in *l*-Si is 5.7. Note that the value for *l*-Si is smaller than that (6.3) reported by Kim et al.[68] It is worth mentioning that the profile with very small death values observed along the diagonal in the Si-centric PD of *l*-Si [Fig. 11(B)], which is rather similar to that of *g*-$Cu_{15}Zr_{85}$,[18] suggesting that the structure of *l*-Si is much more densely packed than that of *a*-Si, stems from the increased density and coordination number. It is presumable from the discussion above that *a*-Si does not exhibit an FSDP as scaled in Fig. 6(B), because the structure of *a*-Si is very different from that of *l*-Si, while there are many similarities in SiO_2 between glassy and liquid phases, as manifested also by a well-defined FSDP.

4. Conclusions

A combination of experimental and computational approaches, with the aid of advanced mathematics, has been realized to reveal the relationship between the diffraction pattern and topology. A systematic analysis of disordered materials with tetrahedral motifs led to the confirmation that the FSDP is not a signature of the formation of a network because an FSDP can be observed in tetrahedral molecular liquids, which do not form a network. Moreover, on the basis of persistent homology analyses, we discussed structural differences in several tetrahedral glassy/amorphous materials and liquids, with a particular focus on silicon and silica. We also addressed the structure modification of liquid phosphorus under high pressures and high temperatures in terms of the diffraction pattern and homology. It is demonstrated that a combination of diffraction data and homology is useful tool for uncovering intermediate-range ordering in disordered materials. This dedicated approach therefore offers a way to gaining crucial knowledge for understanding the nature of disordered materials.

Acknowledgments The synchrotron radiation experiments were performed at BL04B2 of SPring-8 with the approval of the Japan Synchrotron Radiation Research Institute (JASRI) (Proposal Nos. 2016A0134, 2016A4502). This research was supported by JST PRESTO, Japan Grant Numbers JPMPR15N4 (to S.K.) and JPMJPR16N6 (to M.S.); the "Materials Research by Information Integration" Initiative (MI^2I) project of the Support Program for Starting Up Innovation Hub from JST (to Y.O., S.K., A.M., S.T. and Y.H.); JST CREST 15656429 (to Y.H.); and JSPS KAKENHI Grant Numbers JP19K05648 (to Y.O.) and JP17H03121 (to A.M.). We thank Mr. T. Harada for experimental assistance in the high-energy XRD measurement on liquid silicon. Discussions with Profs. T. Otomo, T. Usuki, P. S. Salmon, L. Pusztai, and M. Watanabe and with Drs. K. Suzuya, M. Tucker, and A. Zeidler are gratefully appreciated. The authors are grateful to Prof. K. Amiya for providing $Cu_{50}Zr_{50}$ glass ribbons. Profs. S. Roorda, E. Bychkov, and S. Hosokawa and Drs. A. C. Hannon and Y. Katayama are thanked for providing us with the experimental diffraction data.

References

1) P. A. Egelstaff, *Adv. Chem. Phys.*, 53, 1–6 (1983).
2) S. Kohara and P. S. Salmon, *Adv. Phys.: X*, 1, 640–660 (2016).
3) S. Kohara, *J. Ceram. Soc. Jpn.*, 125, 799–807 (2017).
4) P. S. Salmon, R. A. Martin, P. E. Mason and G. J. Cuello, *Nature*, 435, 75–78 (2005).
5) A. C. Wright and A. J. Leadbetter, *Phys. Chem. Glasses*, 17, 122–145 (1976).
6) J. C. Phillips, *J. Non-Cryst. Solids*, 43, 4337–4377 (1981).
7) D. L. Price, S. C. Moss, R. Reijers, M.-L. Saboungi and S. Susman, *J. Phys. C Solid State*, 21, L1069–L1072 (1988).
8) S. R. Elliott, *Nature*, 354, 445–452 (1991).
9) A. C. Wright, *J. Non-Cryst. Solids*, 179, 84–115 (1994).
10) P. S. Salmon, *Proc. R. Soc. Lon. Ser.-A*, 445, 351–365 (1994).
11) Q. Mei, C. J. Benmore, S. Sen, R. Sharma and J. Yargar, *Phys. Rev. B*, 78, 144204 (2008).
12) W. H. Zachariasen, *J. Am. Chem. Soc.*, 54, 3841–3851 (1932).
13) S. Kohara, J. Akola, L. Patrikeev, M. Ropo, K. Ohara, M. Itou, A. Fujiwara, J. Yahiro, J. T. Okada, T. Ishikawa, A. Mizuno, A. Masuno, Y. Watanabe and T. Usuki, *Nat. Commun.*, 5, 5892–5898 (2014).
14) A. Zeidler and P. S. Salmon, *Phys. Rev. B*, 93, 214204 (2016).
15) R. Shi and H. Tanaka, *Sci. Adv.*, 5, 3194 (2019).
16) S. Le Roux and P. Jund, *Comput. Mater. Sci.*, 49, 70–83 (2010).
17) I. Heimbach, F. Rhiem, F. Beule, D. Knodt, J. Heinen and R. O. Jones, *J. Comput. Chem.*, 38, 389–394 (2017).
18) Y. Hiraoka, T. Nakamura, A. Hirata, E. G. Escobar, K. Matsue and Y. Nishiura, *P. Natl. Acad. Sci. USA*, 113, 7035–7040 (2016).
19) A. Hirata, L. J. Kang, T. Fujita, B. Klumov, K. Matsue, M. Kotani, A. R. Yavari and M. W. Chen, *Science*, 341, 376–379 (2013).
20) P. S. Salmon, *Nat. Mater.*, 1, 87–88 (2002).
21) R. L. McGreevy and L. Pusztai, *Mol. Simulat.*, 1, 359–367 (1988).
22) S. Kohara, K. Ohara, H. Tajiri, C. Song, O. Sakata, T. Usuki, Y. Benino, A. Mizuno, A. Masuno, J. T. Okada, T. Ishikawa and S. Hosokawa, *Z. Phys. Chem.*, 230, 339–368 (2016).
23) S. Kohara, M. Itou, K. Suzuya, Y. Inamura, Y. Sakurai, Y. Ohishi and M. Takata, *J. Phys. Condens. Matter*, 19, 506101 (2007).
24) T. E. Faber and J. M. Ziman, *Philos. Mag.*, 11, 153–173 (1965).
25) S. Plimpton, *J. Comput. Phys.*, 117, 1–19 (1995).
26) O. Greben, P. Jóvári, L. Temleitner and L. Pusztai, *J. Optoelectron. Adv. Mater.*, 9, 3021–3027 (2007).
27) Y. Katayama, T. Mizutani, W. Utsumi, O. Shimomura, M. Yamakata and K.-I. Funakoshi, *Nature*, 403, 170–173 (2000).
28) K. Laaziri, S. Kycia, S. Roorda, M. Chicoine, J. L. Robertson, J. Wang and S. C. Moss, *Phys. Rev. Lett.*, 82, 3460–3463 (1999).
29) T. Kumagai, S. Izumi, S. Hara and S. Sakai, *Comput. Mater. Sci.*, 39, 457–464 (2007).

30) J. Tersoff, *Phys. Rev. B*, 37, 6991–7000 (1988).
31) J. Tersoff, *Phys. Rev. B*, 38, 9902–9905 (1988).
32) M. Murakami, S. Kohara, N. Kitamura, J. Akola, H. Inoue, A. Hirata, Y. Hiraoka, Y. Onodera, I. Obayashi, J. Kalikka, N. Hirao, T. Musso, A. S. Foster, Y. Idemoto, O. Sakata and Y. Ohishi, *Phys. Rev. B*, 99, 045153 (2019).
33) https://www.wpi-aimr.tohoku.ac.jp/hiraoka_labo/homcloud/index.en.html.
34) A. Zeidler, P. S. Salmon, R. A. Martin, T. Usuki, P. E. Mason, G. J. Cuello, S. Kohara and H. E. Fischer, *Phys. Rev. B*, 82, 104208 (2010).
35) E. Bychkov, C. J. Benmore and D. L. Price, *Phys. Rev. B*, 72, 172107 (2005).
36) A. Bytchkov, G. J. Cuello, S. Kohara, C. J. Benmore, D. L. Price and E. Bychkov, *Phys. Chem. Chem. Phys.*, 15, 8487–8494 (2013).
37) A. C. Hannon, D. Di Martino, L. F. Santos and R. M. Almeida, *J. Phys. Chem. B*, 111, 3342–3354 (2007).
38) ISIS Disordered Materials Database, http://www.alexhannon.co.uk/.
39) H. Morita, S. Kohara and T. Usuki, *J. Mol. Liq.*, 147, 182–185 (2009).
40) P. S. Salmon, A. C. Barnes, R. A. Martin and G. J. Cuello, *Phys. Rev. Lett.*, 96, 235502 (2006).
41) A. Zeidler, P. S. Salmon and L. B. Skinner, *P. Natl. Acad. Sci. USA*, 108, 14780–14785 (2011).
42) H. T. J. Reijers, M.-L. Saboungi, D. L. Price, J. W. Richardson, Jr. and K. J. Volin, *Phys. Rev. B*, 40, 6018–6029 (1989).
43) M. Stolz, R. Winter, W. S. Howells and R. L. McGreevy, *J. Phys. Condens. Matter*, 7, 5733–5744 (1990).
44) K. Toukan, H. T. J. Reijers, C.-K. Loong, D. L. Price and M.-L. Saboungi, *Phys. Rev. B*, 41, 11739–11742 (1990).
45) Sz. Pothoczki, L. Temleitner and L. Pusztai, *Chem. Rev.*, 115, 13308–13361 (2015).
46) A. C. Hannon, D. I. Grimley, R. A. Hulme, A. C. Wright and R. N. Sinclair, *J. Non-Cryst. Solids*, 197, 299–316 (1994).
47) A. G. Clare, A. C. Wright, R. N. Sinclair, F. L. Galeener and A. E. Geissberger, *J. Non-Cryst. Solids*, 111, 123–138 (1989).
48) P. H. Gaskell and D. J. Wallis, *Phys. Rev. Lett.*, 76, 66–69 (1996).
49) A. Zeidler, K. Wezka, R. F. Rowlands, D. A. J. Whittaker, P. S. Salmon, A. Polidori, J. W. E. Drewitt, S. Klotz, H. E. Fischer, M. C. Wilding, C. L. Bull, M. G. Tucker and M. Wilson, *Phys. Rev. Lett.*, 112, 135501 (2014).
50) P. S. Salmon, "Magma under Pressure: Advances in High-Pressure Experiments on Structure and Properties of Melts", Ed. by Y. Kono and C. Sanloup, Elsevier, Amsterdam (2018) pp. 347–348.
51) M. Misawa, *J. Chem. Phys.*, 91, 5648–5654 (1989).
52) Sz. Pothoczki, L. Temleitner, P. Jóvári, S. Kohara and L. Pusztai, *J. Chem. Phys.*, 130, 064503 (2009).
53) J. D. Bernal, *Nature*, 183, 170–173 (1959).
54) S. Hosokawa, J. Stellhorn, W.-C. Pilgrim, N. Boudet, N. Blanc, S. Kohara, H. Tajiri, H. Kato, Y. Kawakita and T. Otomo, *JPS Conf. Proc.*, 8, 031002 (2015).
55) P. Lamparter, S. Steeb and E. Grallath, *Z. Naturforsch. C*, 38a, 1210–1222 (1983).
56) C. J. Benmore, R. T. Hart, Q. Mei, D. L. Price, J. Yarger, C. A. Tulk and D. D. Klug, *Phys. Rev. B*, 72, 132201 (2005).
57) J. J. Pluth, J. V. Smith and J. Faber, Jr., *J. Appl. Phys.*, 57, 1045–1049 (1985).
58) K. Kihara, *Eur. J. Mineral.*, 2, 63–77 (1990).
59) L. Levien and C. T. Prewitt, *Am. Mineral.*, 66, 324–333 (1981).
60) P. K. Gupta and A. R. Cooper, *J. Non-Cryst. Solids*, 123, 14–21 (1990).
61) J. P. Rino, I. Ebbsjö, R. K. Kalia, A. Nakano and P. Vashishta, *Phys. Rev. B*, 47, 3053–3062 (1993).
62) S. Kohara, J. Akola, H. Morita, K. Suzuya, J. K. R. Weber, M. C. Wilding and C. J. Benmore, *P. Natl. Acad. Sci. USA*, 108, 14780–14785 (2011).
63) A. Takada, P. Richet, C. R. A. Catlow and G. D. Price, *J. Non-Cryst. Solids*, 345&346, 224–229 (2004).
64) Q. Mei, C. J. Benmore and J. K. R. Weber, *Phys. Rev. Lett.*, 4, 057802 (2007).
65) A. Mizuno, H. Kawauchi, M. Tanno, K. Murai, H. Kobatake, H. Fukuyama, T. Tsukada and M. Watanabe, *ISIJ Int.*, 54, 2120–2124 (2014).
66) G. Urbain, Y. Bottinga and P. Richet, *Geochim. Cosmochim. Ac.*, 46, 1061–1072 (1982).
67) C. A. Angell, *Science*, 267, 1924–1935 (1995).
68) T. H. Kim, G. W. Lee, B. Sieve, A. K. Gangopadhyay, R. W. Hyers, T. J. Rathz, J. R. Rogers, D. S. Robinson, K. F. Kelton and A. I. Goldman, *Phys. Rev. Lett.*, 95, 085501 (2005).